Mineralogical Magazine (2019), **83**, 497–505
doi:10.1180/mgm.2019.1

CAMBRIDGE UNIVERSITY PRESS

Article

Distribution of Cr^{3+} between octahedral and tetrahedral sites in synthetic blue and green $(CaMgSi_2O_6)_{95}(CaCrAlSiO_6)_5$ diopsides

Masahide Akasaka[1]*, Yohei Takasu[1], Makoto Handa[2], Mariko Nagashima[3], Maki Hamada[4] and Terumi Ejima[5]

[1]Department of Geoscience, Graduate School of Science and Engineering, Shimane University, 1060 Nishikawatsu, Matsue 690-8504, Japan; [2]Department of Chemistry, Graduate School of Science and Engineering, Shimane University, 1060 Nishikawatsu, Matsue 690-8504, Japan; [3]Department of Earth Sciences, Graduate School of Sciences and Technology for Innovation, Yamaguchi University, 1677-1 Yoshida, Yamaguchi 753-8512, Japan; [4]School of Natural System, College of Science and Engineering, Kanazawa University, Kanazawa 920-1192, Japan; and [5]Department of Geology, Faculty of Science, Shinshu University, 3–1–1, Asahi, Matsumoto 390–8621, Japan

Abstract

The distribution of Cr^{3+} ions in blue and green diopsides crystallised from a glass with the composition $[CaMgSi_2O_6$ (Di)$]_{95}[CaCrAlSiO_6$ (CrAlTs)$]_5$ (mol.%) was determined using Rietveld refinement of X-ray diffraction data in order to evaluate published results by optical spectroscopic analysis, and to clarify the influence of Cr^{3+}–Al^{3+} distribution between the octahedral *M*1 and tetrahedral *T* sites on the crystal structure. The starting material was $Di_{95}CrAlTs_5$-diopside crystallised from glass at 800°C for 2 days. After another 19 days at 800°C and 1000°C for 7 days, the diopsides remained blue. The blue diopside gradually changed to bluish green by heating at 1200°C for 3 days and to green after 7 days. The stoichiometric compositions of the synthesised phases were confirmed by electron microprobe analysis. The Cr occupancies refined by the Rietveld method resulted in the site populations in the *M*1 and *T* sites: $^{M1}[Mg_{0.95}Cr_{0.030(4)}Al_{0.020}]^{T}[Si_{1.950}Cr_{0.020}Al_{0.030}]$ and $^{M1}[Mg_{0.95}Cr_{0.037(4)}Al_{0.013}]^{T}[Si_{1.950}Cr_{0.013}Al_{0.037}]$ (per 6 oxygens) for the blue diopsides at 800 and 1000°C, respectively: $^{M1}[Mg_{0.95}Cr_{0.042(3)}Al_{0.008}]^{T}[Si_{1.950}Cr_{0.008}Al_{0.042}]$ for the bluish green diopside at 1200°C for 3 days; and $^{M1}[Mg_{0.95}Cr_{0.049(3)}Al_{0.001}]^{T}[Si_{1.950}Cr_{0.001}Al_{0.049}]$ for the green diopside at 1200°C for 7 days. Such Cr and Al distributions effect the volumes and site distortions of the octahedral and tetrahedral coordination polyhedra: the TO_4 tetrahedron volumes of the blue diopsides (2.251–2.258 Å^3) are larger than that of the green diopside (2.237 Å^3); the $M1O_6$ octahedron volumes of the former (11.74–11.77 Å^3) are smaller than that of the latter (11.86 Å^3); the TO_4 tetrahedra in the blue diopside ($<\lambda_{tet}>$ =1.006; $\sigma^2_{\theta(tet)}$ = 24.37–24.69) are less distorted than that of the green diopside ($<\lambda_{tet}>$ = 1.007; $\sigma^2_{\theta(tet)}$ = 27.94); the $M1O_6$ octahedra in the former ($<\lambda_{oct}>$ =1.006; $\sigma^2_{\theta(oct)}$ = 20.39–21.13) are more distorted than that of the latter ($<\lambda_{oct}>$ = 1.005; $\sigma^2_{\theta(oct)}$ = 17.58).

Keywords: chromian diopside, X-ray Rietveld analysis, crystal chemistry of chromium in minerals

(Received 6 August 2018; accepted 26 December 2018; Accepted Manuscript online 12 February 2019; Associate Editor: Andrew G Christy)

Introduction

Clinopyroxene minerals generally contain various transition-metal ions. In calcium clinopyroxenes, Tschermak-type substitutions ($^{VI}M^{2+} + {}^{IV}Si^{4+} \leftrightarrow {}^{VI}M^{3+} + {}^{IV}M^{3+}$) play an essential role in the incorporation of trivalent transition-metal ions. Thus, these clinopyroxenes have been investigated repeatedly in order to understand the: (1) stability of clinopyroxenes with calcium Tschermak-type end-member compositions; (2) solubility of each end-member component in diopside; (3) distribution of trivalent transition-metal ions between octahedral and tetrahedral sites in calcium clinopyroxene; and (4) effect of the Tschermak-type substitutions on the pyroxene structure. Examples of this research in the literature include: synthetic clinopyroxenes in the join $CaMgSi_2O_6$ (diopside: Di)–$CaFe^{3+}AlSiO_6$ (esseneite: Ess) (Hijikata, 1968; Hijikata and Onuma, 1969; Huckenholz *et al.*, 1974; Oba and Onuma, 1978; Ghose *et al.*, 1986; Kurepin *et al.*, 1981; Shinno and Maeda, 1989; and others); in the join Di–$CaFe^{3+}_2SiO_6$ (Huckenholz *et al.*, 1967; Hafner and Huckenholz, 1971); in the join Di–$CaTiAl_2O_6$ ('titan pyroxene': Tp) (Yagi and Onuma, 1967; Onuma *et al.*, 1968); in the join Di–Ess–Tp (Akasaka and Onuma, 1980; Akasaka *et al.*, 1997); in the join Ess–Tp (Onuma and Akasaka, 1980; Akasaka, 1983); in the join Di–Tp–$CaAl_2SiO_6$ (kushiroite: Ksh) (Yang, 1973, 1976; Onuma and Kimura, 1978); in the join Di–Ksh–Ess (Onuma *et al.*, 1981); synthetic $Ca(V^{3+},Al)AlSiO_6$-pyroxene (Ohashi and Sato, 2003) and $CaSc^{3+}AlSiO_6$-pyroxene (Ohashi and Ii, 1978).

As well as the case of clinopyroxenes containing trivalent transition-metal ions, such as Fe^{3+}, V^{3+} and Sc^{3+}, by calcium Tschermak-type substitutions, diopside incorporates Cr^{3+} ions as calcium Tschermak-type $CaCr^{3+}Cr^{3+}SiO_6$ (chromium Tschermak's component: CrTs) or $CaCr^{3+}AlSiO_6$ (chromium–aluminium Tschermak's component: CrAlTs) components. Ikeda and Yagi (1977) determined the maximum solubility of CrTs component in diopside to be 6.7 wt.% at 1 atm and 940°C, and found that the CrTs-bearing diopsides are always blue in colour, in contrast to the green colour of clinopyroxene in the join Di–$NaCrSi_2O_6$ (Ikeda and Yagi 1972; Ikeda and Ohashi, 1974) and natural Cr-bearing diopside (e.g. Naumov *et al.*, 2008).

*Author for correspondence: Masahide Akasaka, Email: akasaka@riko.shimane-u.ac.jp
Cite this article: Akasaka M., Takasu Y., Handa M., Nagashima M., Hamada M. and Ejima T. (2019) Distribution of Cr^{3+} between octahedral and tetrahedral sites in synthetic blue and green $(CaMgSi_2O_6)_{95}(CaCrAlSiO_6)_5$ diopsides. *Mineralogical Magazine* **83**, 497–505. https://doi.org/10.1180/mgm.2019.1

They suggested that the blue colour of the CrTs-bearing diopside is due to tetrahedral Cr^{3+} ions in a low-spin state. The low-spin state of Cr^{3+} ions in CrTs-bearing diopside was proven using magnetic susceptibility measurements by Ikeda and Yagi (1978). Furthermore, Ikeda and Yagi (1982) synthesised diopsides in the join Di–CrAlTs from glasses containing a CrAlTs component up to 5 wt.% (4.48 mol.%), based on the estimated maximum solubility of the CrAlTs component in diopside of ca. 14 wt.% (ca. 13 mol.%) at 1200°C and 1 atm after Dickey *et al.* (1971), and found that $Di_{99}CrAlTs_1$-, $Di_{97}CrAlTs_3$-, and $Di_{95}CrAlTs_5$-diopsides crystallised at temperatures <1160°C are blue in colour, whereas those synthesised at temperatures >1160°C are green in colour. According to the results of the crystal field spectral analysis of the CrAlTs-bearing diopsides by Ikeda and Yagi (1982), both octahedrally coordinated high-spin (HS) and tetrahedrally coordinated low-spin (LS) Cr^{3+} ions are present in the blue diopside, whereas, in the green diopside, nearly all Cr^{3+} ions are in the HS state and are present in the octahedral sites. Moreover, they indicated that the occupancy of Cr^{3+} at the tetrahedral sites decreases with increasing crystallisation temperature from 800°C to 1160°C, and drops to nearly zero at 1160°C.

However, different interpretations for the cause of the blue colour of Cr-bearing diopside have also been proposed: Dickey *et al.* (1971) and Mao *et al.* (1972) explained that the blue colour of the synthetic blue diopside is mainly due to the valence change of Cr^{3+} ions to Cr^{2+}; Schreiber (1977, 1978) and Burns (1993) argued that the blue colour is due to Cr^{4+} ions. Therefore, in order to solve the discrepancy of the above views on the cause of the blue colour of synthetic Cr-bearing diopside, additional data on the distribution of Cr^{3+} ions in the octahedral and tetrahedral sites of Cr^{3+}-bearing diopside is required. No structural evidence of different distribution of Cr^{3+} ions in the octahedral and tetrahedral sites between the blue and green diopsides has been reported because of the lack of structural data on the CrAlTs-bearing diopsides. The purpose of our investigation is to determine the distribution of Cr^{3+} in the CrAlTs-bearing diopside by powder X-ray diffraction for comparison with the results from crystal field spectroscopy in Ikeda and Yagi (1982), and to clarify the influence of Cr^{3+} and Al^{3+} distribution between the octahedral and tetrahedral sites on the crystal structure. In order to achieve this aim, a diopside with a composition of $Di_{95}CrAlTs_5$ (mol.%) was crystallised at 800, 1000 and 1200°C from glass of this composition, and its crystal structure was refined using Rietveld refinement of the powder X-ray diffraction data.

Experimental method

Samples

In the present study, a CrAlTs-bearing diopside with a composition of $Di_{95}CrAlTs_5$ in mol.% was synthesised from a glass with this composition, for two reasons: (1) the quantity of Cr in this composition is enough for the determination of Cr population in the octahedral and tetrahedral sites in the diopside structure; and (2) the results from the CrAlTs-bearing diopside with this composition can be compared with that of $Di_{95}CrAlTs_5$ (in wt.%)-diopside in Ikeda and Yagi (1982).

Reagent-grade chemicals $CaCO_3$, MgO, Al_2O_3, and Cr_2O_3, and synthetic pure cristobalite were used as the source materials. $CaCO_3$ and Cr_2O_3 were dried at 110°C for 24 hr, and MgO and Al_2O_3 were ignited at 1400 and 1350°C, respectively, for 3 hr. Cristobalite was produced by heating of a regent grade amorphous SiO_2 at 1350°C for 3 hr and then rapid cooling. A mixture consisting of synthetic cristobalite and $CaCO_3$, MgO, Al_2O_3, and Cr_2O_3, formulated with a composition of $Di_{95}CrAlTs_5$ in mol.%, was melted in air in a Pt-crucible at 1590–1600°C using a SILICONIT high-temperature Muffle furnace with an electronic temperature controller (Department of Geoscience, Shimane University). Homogenous glass was obtained after two fusions with intermediate quenching and grinding. The glass exhibits a green colour (Fig. 1*a*) and has the same chemical composition as the oxide mixture with $Di_{95}CrAlTs_5$ (mol.%) composition within the experimental and analytical error (Table 1). Powdered glass was crystallised at 800°C in air for 2 days using a Muffle furnace, with a heating element of Kanthal heating wire and an electronic temperature controller (Department of Geoscience, Shimane University). The product was a single-phase of blue diopside with a trace amount of wollastonite-2*M*, and was used as a starting material for the heating experiments at 800, 1000 and 1200°C.

By heating the starting material at 800°C for another 19 days, the run product at 800°C was obtained. The run products at 1000 and 1200°C were obtained by heating of the starting material for 7 days.

Chemical analysis

The chemical compositions of the glass and the diopsides were analysed using a JEOL JXA-8530F field emission electron microprobe analyser (EMPA) at the Department of Geoscience, Shimane University. The EMPA was operated at an accelerating voltage of 15 kV with a beam current of 20 nA and a beam diameter of 1 μm. Standard materials used were synthetic oxides: SiO_2 for Si, Al_2O_3 for Al, Cr_2O_3 for Cr, and MgO for Mg; and synthetic $CaSiO_3$ for Ca. The *ZAF* method was applied for data correction.

Crystal field spectra measurement

In order to compare the crystal field spectra of synthetic blue and green diopsides in the present study with those by Ikeda and Yagi (1982), diffused reflectance spectra of the diopsides in the 300–1600 nm region were measured with a Shimadzu UV-vis-NIR Recording Spectrophotometer Model UV-3100, equipped with an integrating sphere, at the Department of Material Science, Shimane University. Reflectance spectra were plotted against the semi-absorbance scale.

Powder X-ray diffraction data collection and Rietveld analysis

Each fine powder sample of the diopside synthesised at 800, 1100 and 1200°C was mounted in a glass holder with a 20 mm × 18 mm × 0.5 mm cavity by loading the powder from the front of the holder.

Powder X-ray diffraction data were collected using a RIGAKU RINT diffractometer system at the Department of Geoscience, Shimane University, equipped with 1° divergence and scatter slits, a 0.15 mm receiving slit and a curved graphite diffracted-beam monochromator. The Cu X-ray tube generator was operated at 35 kV and 25 mA. For phase identification, the powder X-ray diffraction pattern was taken between 5° and 60° in 2θ using the continuous scan mode with a scan speed of 2° in 2θ per minute. The X-ray diffraction data for Rietveld analysis were measured between 5° and 120° in 2θ using the step-scan mode with a step interval of 0.02° and a step counting time of 4 s.

https://doi.org/10.1180/mgm.2019.1 Published online by Cambridge University Press

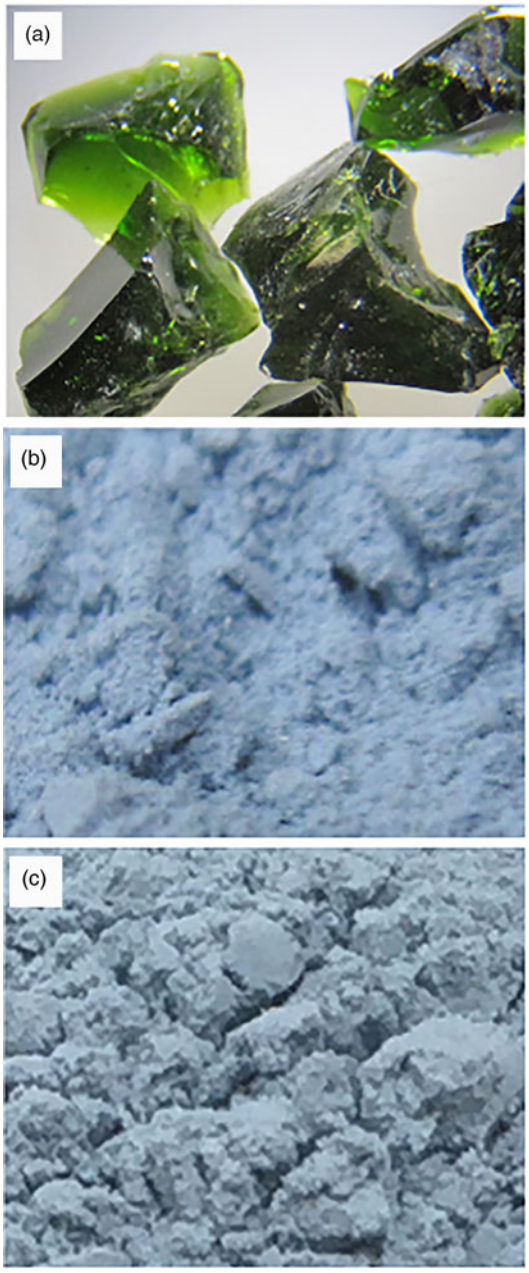

Fig. 1. Photographs of the glass and synthetic diopsides with $Di_{95}CrAlTs_5$ composition: (*a*) glass; (*b*) $Di_{95}CrAlTs_5$-diopside synthesised at 800°C for 19 days of Run No. 1; (*c*) 1000°C for 7 days of Run No. 2; (*d*) 1200°C for 3 days of Run No. 3; and (*e*) 1200°C for 7 days of Run No. 4. Width of view = 1 cm.

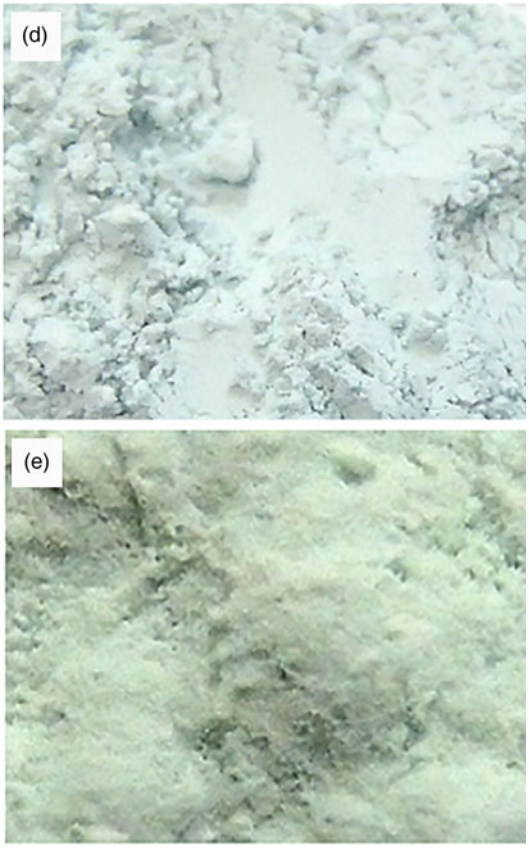

Fig. 1. Continued.

Table 1. EMPA data (wt.%) of a glass prepared from an oxide mixture with the composition of $Di_{95}CrAlTs_5$ (mol.%)*.

		Glass	
	$Di_{95}CrAlTs_5$ Calculated	Average $n = 7$	S.D.
Wt.%			
SiO_2	54.00	54.12	0.47
Al_2O_3	1.17	1.11	0.05
Cr_2O_3	1.74	1.70	0.07
MgO	17.57	17.57	0.15
CaO	25.74	26.09	1.08
Total	100.00	100.59	
Cations per 6 oxygens			
Si	1.95	1.952	0.017
Al	0.05	0.047	0.002
Cr^{3+}	0.05	0.048	0.002
Mg	0.95	0.944	0.009
Ca	1.00	1.008	0.04
Total		3.999	

* Di: $CaMgSi_2O_6$ component; CrAlTs: $CaCr^{3+}AlSiO_6$ component.

The crystal structure was refined using the Rietveld program *RIETAN-FP* (Izumi and Momma, 2007). The peaks were defined using the 'Modified split pseudo-Voigt' function in the *RIETAN-FP* program. The preferred orientation was corrected with the March–Dollase function (Dollase, 1986). A nonlinear least-squares calculation using the Marquardt method was followed by the conjugate-direction method to check the convergence at a local minimum (Izumi, 1993). The *VESTA* program of Momma and Izumi (2011) was used for calculation of the distortion parameters defined by Robinson *et al.* (1971) and the volumes of octahedral and tetrahedral coordination polyhedra. The quadratic elongation parameter $\langle\lambda_{tet}\rangle$ of the TO_4-tetrahedron is defined as $\langle\lambda_{tet}\rangle = \sum_{i=1}^{4} (l_i/l_0)^2/4$ (l_i is the length of the line in the strained state; l_0 is the centre-to-vertex distance for an tetrahedron with *D4h* symmetry whose volume is equal to that of the strained tetrahedron with bond lengths l_i); the variance of the tetrahedral angle as $\sigma^2_{\theta(tet)} = \sum_{i=1}^{6} (\theta_i - 109.47^\circ)^2/5$ (θ_i; O–*T*–O angle); the quadratic elongation parameter $\langle\lambda_{oct}\rangle$ of the $M1O_6$-octahedron is defined as $\langle\lambda_{oct}\rangle = \sum_{i=1}^{6} (l_i/l_0)^2/6$ (l_i is the length of the line in the strained state; l_0 is the centre-to-vertex distance for an octahedron with O_h symmetry whose volume is equal to that of the

https://doi.org/10.1180/mgm.2019.1 Published online by Cambridge University Press

Table 2. Run products* at 800, 1000 and 1200°C in air.

Run No.	Temperature (°C)	Duration (days)	Products
1	800	19	Blue diopside (+ trace wollastonite-2*M*)
2	1000	7	Blue diopside (+ trace wollastonite-2*M*)
3	1200	3	Bluish green diopside (+ trace wollastonite-2*M*)
4	1200	7	Green diopside (+ trace wollastonite-2*M*)

* Starting material: Blue diopside crystallised from the $Di_{95}CrAlTs_5$-glass at 800°C for 2 days.

strained octahedron with bond lengths l_i); and the variance of the octahedral angle is defined as $\sigma^2_{\theta(oct)} = \sum_{i=1}^{12} (\theta_i - 90^\circ)^2/11$ (θ_i; O–*M*1–O angle).

Results

Samples

The run product obtained by heating the blue diopside starting material at 800°C for 19 days was blue in colour (Table 2 Run No. 1; Fig. 1*b*). The product at 1000°C for 7 days also remained blue (Table 2 Run No. 2; Fig. 1*c*). By heating the blue diopside starting material at 1200°C, the blue diopside changed to a bluish green product after 3 days (Table 2 Run No. 3; Fig. 1*d*) and to green after 7 days (Table 2 Run No. 4; Fig. 1*e*). Using powder X-ray diffraction analysis, all products were identified as a diopside single phase with trace amounts of wollastonite-2*M* (Table 2).

The crystal field spectra of the blue diopsides synthesised at 800 and 1000°C (Nos. 1 and 2 in Fig. 2, respectively) and of the green diopside at 1200°C (No. 3 in Fig. 2) resemble those of the blue and green $Di_{95}CrAlTs_5$-diopsides (in wt.%) reported by Ikeda and Yagi (1982), respectively.

All diopsides have a stoichiometric composition of $Di_{95}CrAlTs_5$ within the experimental and analytical errors (Table 3).

X-ray Rietveld analysis

The Rietveld analysis of the X-ray diffraction data was carried out for the diopsides crystallised at 800, 1000 and 1200°C. As a trace amount of wollastonite-2*M* was detected in the run products, the Rietveld refinement was performed for both diopside and wollastonite-2*M*. Details of the X-ray data collection are listed in Table 4. The X-ray single-crystal structural data of diopside with a space group *C*2/*c* by Cameron *et al.* (1973) and of wollastonite-2*M* with $P2_1/a$ by Trojer (1968) were used as structural models of these minerals for the Rietveld refinement. As shown in Table 4, the run products consisted of diopside with mass fractions of 96.8–99.9 wt.% and wollastonite-2*M* with 0.1–3.2 wt.%, indicating that the products essentially consist of single-phase diopside. In the structural refinement, occupancies of Ca at the 8-coordinated *M*2 site, Mg at the octahedral *M*1 site and Si at the tetrahedral *T* site were fixed to 1.0, 0.95 and 0.975, respectively, because diopside in each run product has a stoichiometric chemical composition of $Di_{95}CrAlTs_5$ (mol.%). Site occupancies of Cr and Al in the *M*1 and *T* sites were refined using the following constraints: Al(*M*1) = 1.0 – Mg(*M*1) – Cr(*M*1), Cr(*T*) = [0.05 – Cr(*M*1)]/2, and Al(*T*) = 1.0 – Si(*T*) – Cr(*T*). The atomic positions and isotropic atomic displacement parameters of the wollastonite-2*M* were fixed to the initial values. The refined unit-cell parameters, *R*-factors, goodness-of-fit ($S = R_{wp}/R_e$) and the Durbin-Watson *d* statistic are shown in Table 4, and the observed and calculated powder X-ray diffraction patterns of the samples are given in Fig. 3.

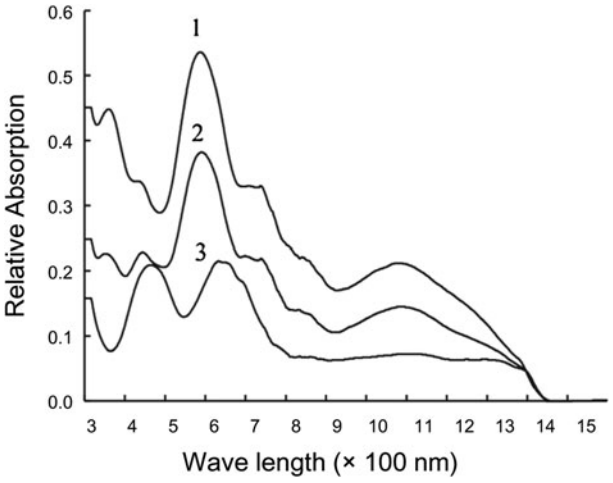

Fig. 2. Crystal field spectra of blue diopside of: (1) Run No.1 at 800°C for 19 days; (2) blue diopside of Run No. 2 at 1000°C for 7 days; and (3) green diopside of Run No. 4 at 1200°C for 7 days.

Table 3. EMPA data (wt.%) of the synthesised diopside solid solutions.

Run No.	No. 1		No. 2		No. 4	
Temperature	800°C		1000°C		1200°C	
Specimen	Blue diopside		Blue diopside		Green diopside	
	Average *n* = 10	S.D.	Average *n* = 10	S.D.	Average *n* = 10	S.D.
Wt.%						
SiO_2	54.04	0.52	54.04	0.28	54.07	0.31
Al_2O_3	1.13	0.08	1.19	0.03	1.23	0.06
Cr_2O_3	1.71	0.11	1.71	0.05	1.74	0.05
MgO	17.55	0.28	17.33	0.25	17.51	0.23
CaO	25.31	0.37	25.51	0.22	25.77	0.13
Total	99.74		99.77		100.32	
Cations per 6 oxygens						
Si	1.961	0.008	1.961	0.008	1.953	0.006
Al	0.048	0.003	0.052	0.004	0.053	0.002
Cr^{3+}	0.049	0.003	0.049	0.002	0.050	0.001
Mg	0.949	0.018	0.938	0.012	0.943	0.011
Ca	0.984	0.012	0.992	0.008	0.997	0.006
Total	3.991		3.992		3.995	

The refined site occupancies, atomic positions and atomic displacement parameters of the $Di_{95}CrAlTs_5$-diopsides crystallised at 800, 1000 and 1200°C are shown in Table 5, and selected bond lengths are given in Table 6. Errors are shown by estimated standard deviations of 1σ.

Resulting site occupancies in the *M*1 and *T* sites of the $Di_{95}CrAlTs_5$-diopside are: (1) $^{M1}[Mg_{0.95}Cr_{0.030(4)}Al_{0.020}]$ and $^{T}[Si_{0.975}Cr_{0.010}Al_{0.015}]$ for the blue diopside of Run No. 1 at 800°C for 19 days; (2) $^{M1}[Mg_{0.95}Cr_{0.037(4)}Al_{0.013}]$ and $^{T}[Si_{0.975}Cr_{0.0066}Al_{0.0184}]$ for the blue diopside of Run No. 2 at 1000°C for 7 days; (3) $^{M1}[Mg_{0.95}Cr_{0.042(3)}Al_{0.008}]$ and $^{T}[Si_{0.975}Cr_{0.004}Al_{0.021}]$ for the bluish green diopside of Run No. 3 at 1200°C for 3 days; and (4) $^{M1}[Mg_{0.95}Cr_{0.049(3)}Al_{0.001}]$ and $^{T}[Si_{0.975}Cr_{0.0006}Al_{0.0244}]$ for the green diopside of Run No. 4 at 1200°C for 7 days. These site occupancies result in the following site populations in the *M*1 and *T* sites: (1) $^{M1}[Mg_{0.95}Cr_{0.030(4)}Al_{0.020}]^{T}[Si_{1.950}Cr_{0.020}Al_{0.030}]$ in atoms per formula unit (O = 6) for the blue diopside of Run No. 1;

https://doi.org/10.1180/mgm.2019.1 Published online by Cambridge University Press

Table 4. Details of data collection and structure refinement*.

Run No.	No. 1		No. 2		No. 3		No. 4	
Run condition	800°C for 19 days		1000°C for 7 days		1200°C for 3 days		1200°C for 7 days	
Specimen	Blue diopside		Blue diopside		Bluish green diopside		Green diopside	
2θ scan range (°) (Cu*K*α)	5–120		5–120		5–120		5–120	
Step interval (°2θ)	0.02		0.02		0.02		0.02	
Counting time/step (s)	4		4		4		4	
Max. intensity (counts)	5040		5507		7109		7288	
Phases	Diopside	Woll.-2*M*	Diopside	Woll.-2*M*	Diopside	Woll.-2*M*	Diopside	Woll.-2*M*
Crystal system	Monoclinic	Monoclinic	Monoclinic	Monoclinic	Monoclinic	Monoclinic	Monoclinic	Monoclinic
Space group	*C*2/*c*	$P2_1/a$	*C*2/*c*	$P2_1/a$	*C*2/*c*	$P2_1/a$	*C*2/*c*	$P2_1/a$
a (Å)	9.7476(3)	15.400(4)	9.7421(2)	15.408(5)	9.7420(3)	15.400(6)	9.7421(2)	15.385(11)
b (Å)	8.9322(3)	7.319(2)	8.9402(2)	7.310(2)	8.9320(3)	7.291(2)	8.9343(1)	7.290(5)
c (Å)	5.2574(2)	7.041(1)	5.2531(1)	7.038(1)	5.2539(2)	7.072(2)	5.2542(1)	7.029(3)
β (°)	106.040(2)	95.09(2)	105.999(2)	95.22(2)	105.945(2)	95.28(3)	105.911(1)	95.25(5)
V (Å^3)	439.93(26)	790.4(16)	439.80(21)	789.4(15)	439.58(23)	786.2(21)	439.80(16)	784.9(36)
Z	4	12	4	12	4	12	4	12
D_{calc} (g/cm^3)	3.290	2.928	3.291	2.932	3.292	2.944	3.291	2.949
Mass fraction	0.999	0.001	0.968	0.032	0.978	0.022	0.991	0.009
R_B (%)	2.23	6.23	2.44	6.01	1.59	3.76	1.48	9.88
R_F (%)	1.31	1.86	1.13	1.39	0.80	1.07	0.86	1.40
R_p (%)	7.27		7.93		6.92		7.33	
R_{wp} (%)	9.86		10.71		9.17		9.95	
R_e (%)	8.16		8.25		7.22		8.01	
S	1.209		1.298		1.270		1.243	
D–W *d*	1.44		1.20		1.22		1.42	

*Abbreviations: R_p – *R*-pattern; R_{wp} – *R*-weighted pattern; R_e – *R*-expected; *S* – Goodness-of-fit (= R_{wp}/R_e); R_B – *R*-Bragg factor; R_F – *R*-structure factor (Young, 1993). D–W *d* – Durbin–Watson *d* statistic (Hill and Flack, 1987). Woll. – Wollastonite.

(2) $^{M1}[Mg_{0.95}Cr_{0.037(4)}Al_{0.013}]^{T}[Si_{1.950}Cr_{0.0132}Al_{0.0368}]$ for the blue diopside of Run No. 2; (3) $^{M1}[Mg_{0.95}Cr_{0.042(3)}Al_{0.008}]^{T}[Si_{1.950}Cr_{0.008}Al_{0.042}]$ for the bluish green diopside of Run No. 3; and (4) $^{M1}[Mg_{0.95}Cr_{0.049(3)}Al_{0.001}]^{T}[Si_{1.950}Cr_{0.0012}Al_{0.0488}]$ for the green diopside of Run No. 4. The validity of the determined site populations was examined in terms of the electrostatic valence principle after Pauling (1929). In the present study, bond strength s_{ij} (bond valence after Donnay and Allmann, 1970) of the bond between cation *i* and anion *j* was calculated using a correlation between bond strength and bond length (Brown and Altermatt, 1985): $s_{ij} = \exp[(l_o - l_{ij})/B]$, where l_o is the bond valence parameter from Brown and Altermatt (1985) and Brese and O'Keeffe (1991); l_{ij} is the observed bond length between cation *i* and anion *j*; and *B* is 0.37 Å. The valence of cation *i*, V_i, was calculated using the equation after Brown and Shannon (1973), $V_i = \sum_j s_{ij}$. As shown in Table 7, the bond-valence sums of the cation sites, Σ*V*(A), and anion site, Σ*V*(C), for O1 correspond approximately to the oxidation state of the sites. However, the bond-valence sums of O2 and O3 are 1.87–1.88 and 2.10–2.12 valence units (vu), deviating slightly from the ideal oxidation state. Brown and Shannon (1973) previously pointed out that rather low bond-valence sums for O2 (1.87–1.88 vu), and high values for O3 (2.12–2.15 vu), are common in clinopyroxene, and attributed its reason to uncertainties of the bond lengths and to real effects such as the second-nearest neighbours which cannot be explained as yet. In recent studies (e.g. Tribaudino *et al.*, 2018), the characteristic behaviour of O2 and O3 in *C*2/*c* pyroxene structure has been recognised: the highest local disorder of the O3 oxygen; limitations of the increase in Si–O3 bond distances by kinking limiting the tetrahedral and octahedral chains; and the under-bonded O2 oxygen atoms. The deviation of the bond-valence sums of O2 and O3 from the ideal oxidation state may be due to the state of oxygen atoms at the O2 and O3 positions.

The distortion parameters defined by Robinson *et al.* (1971) and the volumes of octahedral and tetrahedral coordination polyhedra in the blue and green diopsides are shown in Table 8 with four significant digits based on the accuracy of the bond lengths (Table 6). The TO_4 tetrahedron in the blue diopside has larger volume and more regular form than that in the green diopside, whereas the $M1O_6$ octahedron of the blue diopside is smaller in volume and more distorted than that of the green diopside.

Discussion

Site populations of Cr^{3+} ions in the octahedral and tetrahedral sites

The interpretation that the blue colour of the synthetic blue diopside is mainly due to the valence change of chromium from a trivalent to divalent state was suggested by Dickey *et al.* (1971) and was supported by the crystal field spectroscopic study of Mao *et al.* (1972). Burns (1993) also mentioned that energies of several absorption bands measured by Mao *et al.* (1972) and Ikeda and Yagi (1982) for Cr-bearing blue diopsides are similar to those observed for aqueous Cr^{2+} ions. However, the Cr^{2+} ion is stable only at very low oxygen fugacity conditions at high temperatures (Ikeda and Yagi, 1977) and/or at very high pressures and low oxygen fugacity conditions (Burns, 1975). Thus, Cr^{2+} ions are not stable in the Cr-bearing blue diopsides synthesised in air at 1 atm. On the other hand, Schreiber (1977, 1978) interpreted that the blue colour of Cr-bearing diopside synthesised in his study is due to Cr^{4+} ions. Burns (1993) agreed with the Schreiber's interpretation, because: (1) the Cr^{4+} ion with the $3d^2$ configuration has relatively high crystal field stabilisation energy (CFSE) in the tetrahedral coordination; and (2) the tetrahedral ionic radius of Cr^{4+} (0.41 Å, Shannon, 1976), is

https://doi.org/10.1180/mgm.2019.1 Published online by Cambridge University Press

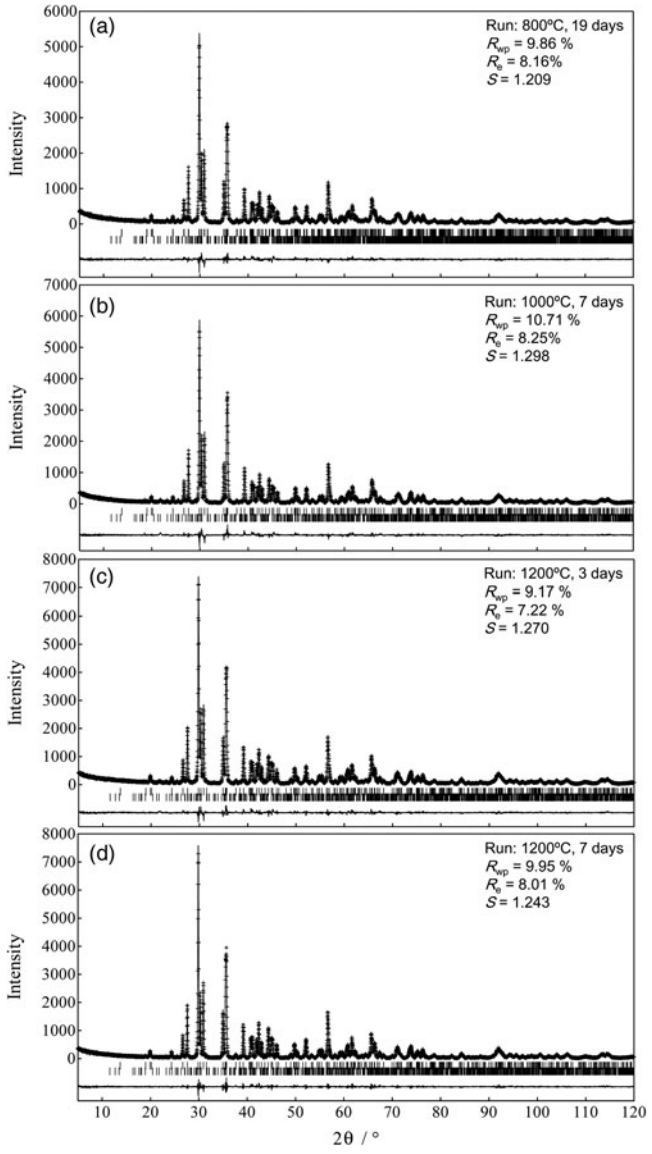

Fig. 3. Observed and calculated powder X-ray diffraction patterns for the run products of: (*a*) Run No. 1 at 800°C for 19 days; (*b*) Run No. 2 at 1000°C for 7 days; (*c*) Run No. 3 at 1200°C for 3 days; and (*d*) Run No. 4 at 1200°C for 7 days. The crosses are the observed data, the solid line is the calculated pattern, and the vertical bars mark all possible Bragg reflections ($K\alpha_1$ and $K\alpha_2$) for diopside with space group *C*2/*c* (upper bars) and wollastonite-2*M* with space group $P2_1/a$ (lower bars). The difference between the observed and calculated pattern is shown at the bottom.

comparable to that of Al^{3+} (0.39 Å). However, as the blue diopside synthesised by Schreiber (1977) was crystallised from glasses with chemical compositions deviating from pyroxene stoichiometry, the consistency between the Cr distribution in his synthetic blue diopside and the estimated oxidation state of Cr cannot be evaluated in terms of the pyroxene composition and its stoichiometry.

Schreiber (1977) and Burns (1993) envisaged that Cr^{3+} enters preferentially into the octahedral sites of diopside but not into the tetrahedral sites. However, Ikeda and Yagi (1977) proved a distribution of Cr^{3+} between the octahedral and tetrahedral sites by successful synthesis of stoichiometric CrTs-bearing blue diopside. Moreover, based on the crystal field spectroscopic data of the diopsides in the joins Di–CrTs (Ikeda and Yagi, 1977) and Di–CrAlTs (Ikeda and Yagi, 1982) and magnetic susceptibility data for CrTs-bearing diopside (Ikeda and Yagi, 1978), Ikeda and Yagi (1982) found that the Cr^{3+} ions in the tetrahedral sites are in the low-spin state, and concluded that the blue colour

Table 5. Site occupancies (occ.), atomic coordinates (*x*, *y*, *z*) and isotropic atomic displacement parameters (U_{eq} in Å^2) of the synthesised diopsides.

Site	Wyk.*		Run No. 1 800°C for 19 days Blue diopside	Run No. 2 1000°C for 7 days Blue diopside	Run No. 3 1200°C for 3 days Bluish green diopside	Run No. 4 1200°C for 7 days Green diopside
*M*2	4*e*	*x*	0	0	0	0
		y	0.3000(2)	0.3002(2)	0.3008(2)	0.3013(2)
		z	¼	¼	¼	¼
		U_{eq}	0.0101(15)	0.0112(6)	0.0099(14)	0.0085(5)
		occ.	Ca 1.0	Ca 1.0	Ca 1.0	Ca 1.0
*M*1	4*e*	*x*	0	0	0	0
		y	0.9078(3)	0.9075(3)	0.9082(2)	0.9084(2)
		z	¼	¼	¼	¼
		U_{eq}	0.0067(18)	0.0039(10)	0.0042(15)	0.0063(8)
		occ.	Mg 0.95	Mg 0.95	Mg 0.95	Mg 0.95
			Cr 0.030(4)	Cr 0.037(4)	Cr 0.042(3)	Cr 0.049(3)
			Al 0.020	Al 0.013	Al 0.008	Al 0.001
T	8*f*	*x*	0.2867(2)	0.2866(2)	0.2867(1)	0.2868(1)
		y	0.0939(2)	0.0942(2)	0.0942(2)	0.0939(2)
		z	0.2314(3)	0.2301(3)	0.2295(3)	0.2297(3)
		U_{eq}	0.0069(15)	0.0073(6)	0.0063(1)	0.0062(5)
		occ.	Si 0.975	Si 0.975	Si 0.975	Si 0.975
			Cr 0.010	Cr 0.0066	Cr 0.004	Cr 0.0006
			Al 0.015	Al 0.0184	Al 0.021	Al 0.0244
O1	8*f*	*x*	0.1143(3)	0.1142(3)	0.1149(3)	0.1158(3)
		y	0.0878(4)	0.0872(4)	0.0874(3)	0.0877(3)
		z	0.1444(6)	0.1451(6)	0.1442(5)	0.1425(5)
		U_{eq}	0.0025(18)	0.0018(9)	0.0024(15)	0.0018(8)
O2	8*f*	*x*	0.3619(3)	0.3610(3)	0.3619(3)	0.3621(3)
		y	0.2512(3)	0.2516(3)	0.2510(3)	0.2503(3)
		z	0.3158(6)	0.3141(6)	0.3164(5)	0.3177(5)
		U_{eq}	0.0073(18)	0.0073(10)	0.0068(15)	0.0052(8)
O3	8*f*	*x*	0.3501(4)	0.3507(3)	0.3501(3)	0.3512(3)
		y	0.0195(3)	0.0203(3)	0.0187(3)	0.0184(3)
		z	0.9977(7)	0.9960(7)	0.9955(6)	0.9954(6)
		U_{eq}	0.0034(18)	0.0051(10)	0.0048(16)	0.0045(8)

*Wyk. – Wyckoff site notation.

Table 6. Selected bond lengths (Å).

Run No. Run condition Specimen	No. 1 800°C for 19 days Blue diopside	No. 2 1000°C for 7 days Blue diopside	No. 3 1200°C for 3 days Bluish green diopside	No. 4 1200°C for 7 days Green diopside
*M*2–O1 ×2	2.342(3)	2.346(3)	2.353(3)	2.363(3)
*M*2–O2 ×2	2.352(3)	2.363(3)	2.351(2)	2.346(2)
*M*2–O3 ×2	2.582(3)	2.588(3)	2.576(3)	2.568(3)
*M*2–O3' ×2	2.736(3)	2.720(3)	2.726(2)	2.718(2)
<*M*2–O>	2.503	2.504	2.502	2.498
*M*1–O1 ×2	2.066(3)	2.068(3)	2.066(2)	2.062(2)
*M*1–O1' ×2	2.117(4)	2.112(3)	2.113(3)	2.123(3)
*M*1–O2 ×2	2.036(3)	2.035(3)	2.040(3)	2.046(3)
<*M*1–O>	2.073	2.072	2.073	2.077
T–O1	1.616(3)	1.616(3)	1.611(3)	1.603(3)
T–O2	1.590(3)	1.588(3)	1.588(3)	1.587(2)
T–O3	1.658(3)	1.662(3)	1.663(3)	1.669(3)
T–O3'	1.700(4)	1.705(4)	1.696(3)	1.694(3)
<*T*–O>	1.641	1.643	1.640	1.638

https://doi.org/10.1180/mgm.2019.1 Published online by Cambridge University Press

Table 7. Bond-valence sums (in vu) of blue diopside of Run No. 1 at 800°C, blue diopside of Run No. 2 at 1000°C, bluish green diopside of Run No. 3 at 1200°C and green diopside of Run No. 4 at 1200°C.*

	*M*2	*M*1	*T*	Σ*V*(C)	Anion chemistry
Run No. 1, 800°C					
O1	0.34×2↓	0.37×2↓	1.06	2.09	O^{2-}
O1'		0.32×2↓			
O2	0.33×2↓	0.40×2↓	1.15	1.88	O^{2-}
O3	0.19×2↓		0.96	2.13	O^{2-}
O3'	0.13×2↓		0.85		
Σ*V*(A)	1.98	2.18	4.02		
Run No. 2, 1000°C					
O1	0.34×2↓	0.37×2↓	1.07	2.10	O^{2-}
O1'		0.32×2↓			
O2	0.32×2↓	0.40×2↓	1.15	1.87	O^{2-}
O3	0.19×2↓		0.94	2.10	O^{2-}
O3'	0.13×2↓		0.84		
Σ*V*(A)	1.96	2.18	4.00		
Run No. 3, 1200°C					
O1	0.33×2↓	0.37×2↓	1.08	2.10	O^{2-}
O1'		0.32×2↓			
O2	0.33×2↓	0.39×2↓	1.15	1.87	O^{2-}
O3	0.19×2↓		0.94	2.12	O^{2-}
O3'	0.13×2↓		0.86		
Σ*V*(A)	1.96	2.16	4.03		
Run No. 4, 1200°C					
O1	0.32×2↓	0.37×2↓	1.11	2.11	O^{2-}
O1'		0.32×2↓			
O2	0.34×2↓	0.39×2↓	1.15	1.88	O^{2-}
O3	0.19×2↓		0.93	2.12	O^{2-}
O3'	0.14×2↓		0.86		
Σ*V*(A)	1.98	2.16	4.05		

*Multiplicity is indicated by ×↓. Σ*V*(C) is the valence of bonds reaching anions. Σ*V*(A) is the valence of bonds emanating from cations summed over the bonded anions.

Table 8. Average bond lengths, polyhedral volumes, quadratic elongations and bond angle variances* of TO_4 and $M1O_6$ coordination polyhedra in the synthesised diopsides of Run Nos. 1, 2 and 4.

Run No.	No. 1	No. 2	No. 4
Run condition	800°C for 19 days	1000°C for 7 days	1200°C for 7 days
Specimen	Blue diopside	Blue diopside	Green diopside
***TO*$_4$ tetrahedron**			
Average <*T*–O> bond length (Å)	1.641	1.643	1.638
Polyhedral volume (Å^3)	2.251	2.258	2.237
Quadratic elongation $<\lambda_{tet}>$	1.0057	1.0058	1.0066
Bond angle variance $\sigma_\theta(tet)^2$ (degree^2)	24.37	24.69	27.94
***M*1O$_6$ octahedron**			
Average <*M*1–O> bond length (Å)	2.073	2.072	2.077
Polyhedral volume (Å^3)	11.766	11.743	11.855
Quadratic elongation $<\lambda_{oct}>$	1.0063	1.0064	1.0054
Bond angle variance $\sigma_\theta(oct)^2$ (degree^2)	20.39	21.13	17.58

*Polyhedral volume, quadratic elongation and bond angle variance were calculated using the *VESTA* program (Momma and Izumi, 2011). Quadratic elongation and bond angle variance are defined by Robinson *et al.* (1971). The definitions are given in the text.

of the CrTs- and CrAlTs-bearing diopsides is due to tetrahedral LS Cr^{3+}. As the crystal field spectra of the blue and green diopsides measured in this study resemble those in Ikeda and Yagi (1982), the results of the crystal field spectroscopic analysis by Ikeda and Yagi (1982) are applicable to the spectra in our study.

Ikeda and Yagi (1982) formulated a determinative curve for the site populations of Cr^{3+} ions in CrAlTs-bearing diopsides from the spectra of CrTs-bearing diopsides given in Ikeda and Yagi (1977), and determined the site populations of Cr^{3+} ions in the octahedral and tetrahedral sites of the CrAlTs-bearing blue diopsides. As shown in Fig. 4, their result on the $Di_{95.52}CrAlTs_{4.48}$ (mol.%)-diopside indicates that the atomic ratio of Cr^{3+} at the tetrahedral site versus total Cr^{3+} is 38 at.% at 800°C, which decreases with increasing temperature and drops down to 2 at.% at temperatures >1160°C. According to our results from Rietveld analysis of the $Di_{95}CrAlTs_5$-diopside, the Cr^{3+} abundances in the tetrahedral sites at the temperatures of 800, 1000 and 1200°C are 40, 26 and 2 at.% of the total Cr^{3+}, respectively; and in contrast, 60, 74 and 98 at.% Cr^{3+} of total Cr^{3+} distribute in the octahedral *M*1 sites at 800, 1000 and 1200°C, respectively (Fig. 4). Therefore, our result is very consistent with, and supports that of Ikeda and Yagi (1982).

Structural difference of the M1O$_6$ octahedra and TO$_4$ tetrahedra between the blue and green Cr^{3+}-bearing diopsides

The distributions of Cr^{3+} and Al^{3+} between the octahedral and tetrahedral sites in the $Di_{95}CrAlTs_5$-diopside affect the volumes of coordination polyhedra. The larger volume of the TO_4 tetrahedron of the blue diopside (2.251 and 2.258 Å^3 at 800 and 1000°C, respectively) than the green diopside (2.237 Å^3 at 1200°C) is attributed to the higher Cr^{3+}:Al^{3+} ratio at the tetrahedral sites of the blue diopside (Cr^{3+}:Al^{3+} = 0.010:0.015 and 0.007:0.018 in occupancy value at 800 and 1000°C, respectively) than the green diopside (Cr^{3+}:Al^{3+} = 0.0006:0.0244 at 1200°C), because the ionic radius of the tetrahedral LS Cr^{3+} ion (0.46 Å, Ikeda and Yagi, 1982), is larger than that of tetrahedral Al^{3+} (0.39 Å). In contrast, the higher Cr^{3+}:Al^{3+} ratio at the *M*1 site in the green diopside (Cr^{3+}:Al^{3+} = 0.049:0.001 in occupancy value) than that in the blue diopside (Cr^{3+}:Al^{3+} = 0.030:0.020 and 0.037:0.013 at 800 and 1000°C, respectively) results in the larger volume of the $M1O_6$ octahedron of the green diopside (11.86 Å^3) than that of the blue diopside (11.77 and 11.74 Å^3 at 800 and 1000°C, respectively).

The site distortions of the $M1O_6$ octahedron and TO_4 tetrahedron are also influenced by the distributions of Cr^{3+} and Al^{3+} in the octahedral and tetrahedral sites. The TO_4 tetrahedron in the blue diopside with $<\lambda_{tet}>$ =1.006 and $\sigma^2_{\theta(tet)}$ = 24.37–24.69 is more regular in form than that of the green diopside with $<\lambda_{tet}>$ = 1.007 and $\sigma^2_{\theta(tet)}$ = 27.94, whereas the $M1O_6$ octahedron in the blue diopside with $<\lambda_{oct}>$ =1.006 and $\sigma^2_{\theta(oct)}$ = 20.39–21.13 is more distorted than that of the green diopside with $<\lambda_{oct}>$ = 1.005 and $\sigma^2_{\theta(oct)}$ = 17.58 (Table 8). Therefore, the structural properties of the $Di_{95}CrAlTs_5$-diopside are well correlated with the distributions of Cr^{3+} and Al^{3+} between the octahedral and tetrahedral sites.

Ikeda and Yagi (1982) found that transformation of LS Cr^{3+} ions of the tetrahedral site to HS ones of the octahedral site is attained at 1160°C, and suggested that the rearrangement of Cr^{3+} and Al^{3+} ions between the octahedral and tetrahedral sites in the CrAlTs-bearing diopside depends on the kinetics of diffusion of Cr^{3+} and Al^{3+} ions in the specimens. In our heating experiment on blue diopside at 1200°C for 3 days, the colour and the Cr^{3+}–Al distribution between the octahedral and tetrahedral sites changed to an intermediate state between the blue and green diopsides (Figs 1 and 4). Such gradual change from the blue diopside to the green diopside with increasing run durations at 1200°C is consistent with Ikeda and Yagi's suggestion.

https://doi.org/10.1180/mgm.2019.1 Published online by Cambridge University Press

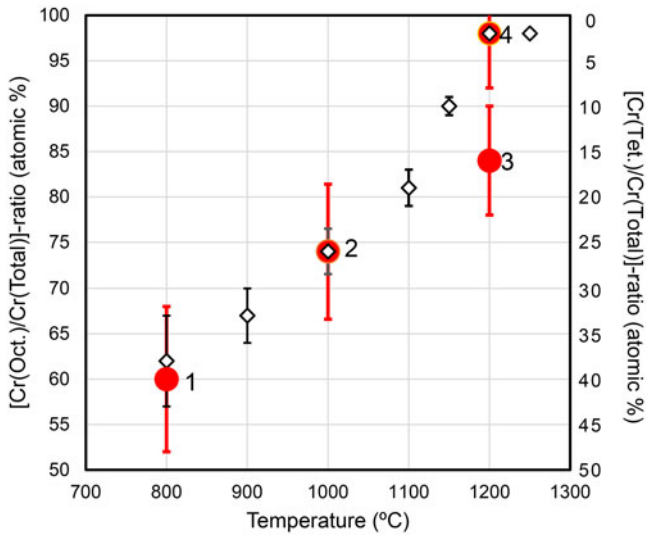

Fig. 4. Ratios of Cr abundance at the octahedral and tetrahedral sites against total Cr in $Di_{95}CrAlTs_5$ (mol.%)-diopside in this study (red closed circle mark) and $Di_{95}CrAlTs_5$ (wt.%)-diopside after Ikeda and Yagi (1982) (open diamond mark). The numbers 1, 2, 3 and 4 correspond to the run numbers shown in Table 2.

Implications

As explained by Ikeda and Yagi (1982), the reason why Cr-bearing blue diopsides have not been found in natural rocks is due to the slow kinetics of transformation from octahedral HS Cr^{3+} to tetrahedral LS Cr^{3+} on cooling. The lack of driving force from CFSE differences and slowness of the diffusion required for the transformation from octahedral HS Cr^{3+} to tetrahedral LS Cr^{3+} means that Cr-bearing diopside formed at high temperatures retains its Cr^{3+} in octahedral coordination when cooled to ambient temperature, resulting in the green colour. This interpretation is consistent with the experimental results that the green diopside is formed by heating of the blue diopside at temperatures >1160°C but a reverse reaction from the green diopside to the blue diopside has not been successful (Ikeda and Yagi, 1982).

Such behaviour of the Cr^{3+} ion with $3d^3$ configuration is quite different from that of Fe^{3+} with $3d^5$ configuration. In contrast to Cr^{3+}, Fe^{3+} in minerals and chemical compounds is commonly in a HS state (Shannon, 1976), and the translation from HS state to LS state occurs only at the extremely high pressures of lower mantle conditions (e.g. Mashino *et al.*, 2014; Sinmyo *et al.*, 2017); also the case for Fe^{2+} (e.g. Hamada *et al.*, 2016). Moreover, despite the similarity of ionic radii between Fe^{3+} (HS $^{VI}Fe^{3+}$ and HS $^{IV}Fe^{3+}$ are 0.645 and 0.49 Å, respectively) and Cr^{3+} (HS $^{VI}Cr^{3+}$ and LS $^{IV}Cr^{3+}$ are 0.62 and 0.46 Å, respectively), the distribution scheme of Fe^{3+} ions between octahedral and tetrahedral sites is also different from that of Cr^{3+} ions: in clinopyroxene in the join $Di–CaFe^{3+}AlSiO_6$ synthesised at temperatures above 800°C, Fe^{3+} ions distribute not only in the octahedral site but also in the tetrahedral site at ambient temperatures (Kurepin *et al.*, 1981; Akasaka, 1983; Ghose *et al.*, 1986; Shinno and Maeda, 1989; Akasaka *et al.*, 1997). Because the CFSEs of Fe^{3+} at octahedral and tetrahedral sites are zero, the distribution of Fe^{3+} and Al^{3+} between octahedral and tetrahedral sites is not influenced by the crystal field effect, and, thus, is controlled by the volumes of coordination polyhedra and the difference in ionic radii between Fe^{3+} and Al^{3+} (Akasaka *et al.*, 1997). Accordingly, the distinctive behaviour of Cr^{3+} in the diopside structure is attributed to the spin state of Cr^{3+} ions with $3d^3$ configuration and the crystal field effect as well as its ionic radius at the octahedral and tetrahedral sites.

Conclusions

The results of our Rietveld analysis study on the Cr^{3+} distribution between the octahedral and tetrahedral sites in the CrAlTs-bearing blue and green diopsides are consistent with those determined by means of crystal field spectral analysis by Ikeda and Yagi (1982): Cr^{3+} abundance in the tetrahedral sites decreases from 40 at.% of total Cr^{3+} at 800°C to 2 at.% of total Cr^{3+} at 1200°C through 26 at.% at 1000°C; in contrast, 60, 74 and 98 at.% Cr^{3+} of total Cr^{3+} distribute in the octahedral *M*1 sites at 800, 1000 and 1200°C, respectively. Such different Cr^{3+} distribution in the octahedral and tetrahedral sites between the blue and green diopsides causes the difference of the volumes and distortions of the $M1O_6$ and TO_4 polyhedra in these diopsides: the TO_4 tetrahedron in the blue diopside has larger volume and more regular form than that in the green diopside, whereas the $M1O_6$ octahedron of the blue diopside is smaller in volume and more distorted than that of the green diopside.

Acknowledgements. The authors thank Professor Emeritus Dr. Ko Ikeda of Yamaguchi University for his critical reading of the manuscript and valuable comments and for his help with this study, Dr. Fujio Izumi of the National institute for Materials Science, Tsukuba, and Dr. Koichi Momma of the National Museum of Nature and Science, Tokyo, for their permission to use the *RIETAN-FP* and *VESTA* programs. The authors also thank Dr. Stuart Mills, Principal Editor, two anonymous reviewers, and Dr. Helen Kerbey, Production Editor, for critical and constructive comments.

References

Akasaka M. (1983) ^{57}Fe Mössbauer study of clinopyroxenes in the join $CaFe^{3+}AlSiO_6$–$CaTiAl_2O_6$. *Physics and Chemistry of Minerals*, **9**, 205–211.

Akasaka M. and Onuma K. (1980) The join $CaMgSi_2O_6$–$CaFe^{3+}AlSiO_6$–$CaTiAl_2O_6$ and its bearing on the Ti-rich fassaitic pyroxenes. *Contributions to Mineralogy and Petrology*, **71**, 301–312.

Akasaka M., Ohashi H. and Shinno I. (1997) Distribution of trivalent Al, Fe and Ga ions in synthetic calcium Tschermak-type clinopyroxenes. Pp. 166–181 in: *Geochemical Studies on Synthetic and Natural Rock Systems* (A.K. Gupta, K. Onuma and M. Arima, editors). Allied Publishers LTD, New Delhi, India.

Brese N.E. and O'Keeffe M. (1991) Bond-valence parameters for solids. *Acta Crystallographica*, **B47**, 192–197.

Brown I.D. and Altermatt D. (1985) Bond-valence parameters obtained from a systematic analysis of the Inorganic Crystal Structure Database. *Acta Crystallographica*, **A29**, 266–282.

Brown I.D. and Shannon R.D. (1973) Empirical bond-strength–bond-length curves for oxides. *Acta Crystallographica*, **A29**, 266–282.

Burns R.G. (1975) Crystal field effects in chromium and its partitioning in the mantle. *Geochimica Cosmochimica Acta*, **39**, 857–864.

Burns R.G. (1993) *Mineralogical Applications of Crystal Field Theory (Second Edition)*. Cambridge University Press, UK.

Cameron M., Sueno S., Prewitt C.T. and Papike J.J. (1973) High-temperature crystal chemistry of acmite, diopside, hedenbergite, jadeite, spodumene, and ureyite. *American Mineralogist*, **58**, 594–618.

Dickey Jr. J.S., Yoder Jr. H.S. and Schairer J.F. (1971) Chromium in silicate-oxide systems. *Carnegie Institution of Washington, Yearbook*, **70**, 118–122.

Dollase W.A. (1986) Correction of intensities for preferred orientation in powder diffractometry: application of the March model. *Journal of Applied Crystallography*, **19**, 267–272.

Donnay G. and Allmann R. (1970) How to recognize O^{2-}, OH^-, and H_2O in crystal structures determined by X-rays. *American Mineralogist*, **55**, 1003–1015.

Ghose S., Okamura F.P. and Ohashi H. (1986) The crystal structure of $CaFe^{3+}SiAlO_6$ and the crystal chemistry of Fe^{3+}–Al^{3+} substitution in calcium Tschermak's pyroxene. *Contributions to Mineralogy and Petrology*, **92**, 530–535.

Hafner S.S. and Huckenholz H.G. (1971) Mössbauer spectrum of synthetic ferri-diopside. *Nature Physical Science*, **233**, 9–10.

Hamada M., Kamada S., Ohtani E., Mitsui T., Masuda R., Sakamaki T., Suzuki N., Maeda F. and Akasaka M. (2016) Magnetic and spin transitions in wüstite: A synchrotron Mössbauer spectroscopic study. *Physical Review*, **B93**, 155–165.

Hijikata K. (1968) Unit-cell dimensions of the clinopyroxenes along the join $CaMgSi_2O_6$–$CaFe^{3+}AlSiO_6$. *Journal of Faculty of Science, Hokkaido University, Series IV*, **14**, 149–157.

Hijikata K. and Onuma K. (1969) Phase equilibria of the system $CaMgSi_2O_6$–$CaFe^{3+}A1SiO_6$ in air. *Journal of Mineralogy, Petrology and Economic Geology*, **62**, 209–217.

Hill R.J. and Flack H.D. (1987) The use of the Durbin−Watson *d* statistic in Rietveld analysis. *Journal of Applied Crystallography*, **20**, 356–361.

Huckenholz H.G., Schairer J.F. and Yoder Jr. H.S. (1967) Synthesis and stability of ferridiopside. *Carnegie Institution of Washington, Year Book*, **66**, 334–347.

Huckenholz H.G., Lindhuber W. and Springer J. (1974) The join $CaSiO_3$–Al_2O_3–Fe_2O_3 of the CaO–Al_2O_3–Fe_2O_3–SiO_2 quarternary system and its bearing on the formation of granditic garnets and fassaite pyroxenes. *Neues Jahrbuch für Mineralogie – Abhandlungen*, **121**, 160–207.

Ikeda K. and Ohashi H. (1974) Crystal field spectra of diopside-kosmochlor solid solutions formed at 15 kb pressure. *Journal of Japanese Association of Mineralogy, Petrology and Economic Geology*, **69**, 103–109.

Ikeda K. and Yagi K. (1972) Synthesis of kosmochlor and phase equilibria in the join $CaMgSi_2O_6$–$NaCrSi_2O_6$. *Contributions to Mineralogy and Petrology*, **36**, 63–72.

Ikeda K. and Yagi K. (1977) Experimental study on the phase equilibria in the join $CaMgSi_2O_6$–$CaCrCrSiO_6$ with special reference to the blue diopside. *Contributions to Mineralogy and Petrology*, **61**, 91–106.

Ikeda K. and Yagi K. (1978) Reply to H. D. Schreiber. *Contributions to Mineralogy and Petrology*, **66**, 343–344.

Ikeda K. and Yagi K. (1982) Crystal-field spectra for blue and green diopsides synthesized in the join $CaMgSi_2O_6$-$CaCrAlSiO_6$. *Contributions to Mineralogy and Petrology*, **81**, 113–118.

Izumi F. (1993) Rietveld analysis program RIETAN and PREMOS and special applications. Pp. 236–253 in: *The Rietveld Method* (R.A. Young, editor). Oxford Science Publications, UK.

Izumi F. and Momma K. (2007) Three-dimensional visualization in powder diffraction. *Solid State Phenomena*, **130**, 15–20.

Kurepin V.A., Polshin E.V. and Alibekov G.I. (1981) Intracrystalline distribution of iron (3+) and aluminium cations in clinopyroxene ($CaFe^{3+}AlSiO_6$). *Mineralogischeskii Zhurnal*, **3**, 83–88.

Mao H.K., Bell P.M. and Dickey Jr. J.S. (1972) Comparison of the crystal-field spectra of natural and synthetic chrome diopside. *Carnegie Institution of Washington, Yearbook*, **71**, 538–541.

Mashino I., Ohtani E., Hirao N., Mitsui T., Masuda R., Seto M., Sakai T., Takahashi S. and Nakano S. (2014) Chemistry and Mineralogy of Earth's Mantle. The spin state of iron in Fe^{3+}-bearing Mg-perovskite and its crystal chemistry at high pressure. *American Mineralogist*, **99**, 1555–1561.

Momma K. and Izumi F. (2011) VESTA 3 for three-dimensional visualization of crystal, volumetric and morphology data. *Journal of Applied Crystallography*, **44**, 1272–1276.

Naumov V.B., Kamenetsky F.S., Thomas R., Kononkova N.N. and Ryzhenko B.N. (2008) Inclusions of silicate and sulfate melts in chrome diopside from the Inagli Deposit, Yakutia, Russia. *Geochemistry International*, **46**, 554–564.

Oba T. and Onuma K. (1978) Preliminary report of the join $CaMgSi_2O_6$-$CaFe^{3+}AlSiO_6$ at low oxygen fugacity. *Journal of Faculty of Science, Hokkaido University, Series IV*, **18**, 433–444.

Ohashi H. and Ii N. (1978) Structure of $CaScAlSiO_6$ pyroxene. *Journal of Mineralogy, Petrology and Economic Geology*, **73**, 267–273.

Ohashi H. and Sato A. (2003) Crystal structure of $Ca(V_{0.67},Al_{0.33})AlSiO_6$ pyroxene. Pp.83–90 in: *X-ray Study on Si–O Bonding* (H. Ohashi, editor). MARUZEN Publishing Service Center, Tokyo, Japan.

Onuma K. and Akasaka M. (1980) Clinopyroxene with $Si < Al_{IV}$ in the join $CaFeAlSiO_6$–$CaTiAl_2O_6$. *Mineralogical Magazine*, **43**, 851–856.

Onuma K. and Kimura M. (1978) Study of the system $CaMgSi_2O_6$–$CaAl_2SiO_6$–$CaFe^{3+}AlSiO_6$–$CaTiAl_2O_6$: II, The join $CaMgSi_2O_6$–$CaAl_2SiO_6$– $CaTiAl_2O_6$, and its bearing on Ca-Al-rich inclusions in carbonaceous chondrite. *Journal of Faculty of Science, Hokkaido University, Series IV*, **18**, 215–236.

Onuma K., Hijikata K. and Yagi K. (1968) Unit-cell dimensions of synthetic titan-bearing clinopyroxenes. *Journal of Faculty of Science, Hokkaido University, Series IV*, **14**, 111–121.

Onuma K., Akasaka M. and Yagi K. (1981) The bearing of the system $CaMgSi_2O_6$–$CaAl_2SiO_6$–$CaFeAlSiO_6$ on fassaitic pyroxene. *Lithos*, **14**, 173–182.

Pauling L. (1929) The principles determining the structure of complex ionic crystals. *Journal of American Chemical Society*, **51**, 1010–1026.

Robinson K., Gibbs G.V. and Ribbe P.H. (1971) Quadratic elongation: a quantitative measure of distortion in coordination polyhedra. *Science*, **172**, 567–570.

Schreiber H.D. (1977) On the nature of synthetic blue diopside crystals: The stabilization of tetravalent chromium. *American Mineralogist*, **62**, 522–527.

Schreiber H.D. (1978) Chromium, blue diopside, and experimental petrology. A discussion. *Contributions to Mineralogy and Petrology*, **66**, 341–342.

Shannon R.D. (1976) Revised effective ionic radii and systematic studies of interatomic distances in halides and chalcogenides. *Acta Crystallographica*, **A32**, 751–767.

Shinno I. and Maeda Y. (1989) Mössbauer spectra of diopside containing 4- and 6-coordinated ferric irons at 78 K and 4.2 K. *Mineralogical Journal*, **14**, 191–197.

Sinmyo R., McCammon C. and Dubrovinsky L. (2017) The spin state of Fe^{3+} in lower mantle bridgmanite. *American Mineralogist*, **102**, 1263–1269.

Tribaudino M., Mantovani L., Mezzadri F., Calestani G. and Bromiley G. (2018) The structure of $P2_1/c$ $(Ca_{0.2}Co_{0.8})CoSi_2O_6$ pyroxene and the $C2/c$ - $P2_1/c$ phase transition in natural and synthetic pyroxenes. *Mineralogical Magazine*, **82**, 211–228.

Trojer F.J. (1968) The crystal structure of parawollastonite. *Zeitschrift für Kristallographie*, **127**, 290–308.

Yagi K. and Onuma K. (1967) The system $CaMgSi_2O_6$–$CaTiAl_2O_6$ and its bearing on the titanaugite. *Journal of Faculty of Science, Hokkaido University, Series IV*, **13**, 463–483.

Yang H.Y. (1973) Synthesis of an Al- and Ti-rich clinopyroxene in the system $CaMgSi_2O_6$–$CaAl_2SiO_6$–$CaTiAl_2O_6$. *EOS*, **54**, 478.

Yang H.Y. (1976) The join $CaMgSi_2O_6$–$CaAl_2SiO_6$–$CaTiAl_2O_6$ and its bearing on the origin of the Ca- and Al-rich inclusion in the meteorites. *Proceedings of the Geological Society of China*, **19**, 107–126.

Young R.A. (1993) Introduction to the Rietveld method. Pp. 1–38 in: *The Rietveld Method* (Young R.A. editor). Oxford Science Publications, UK.

https://doi.org/10.1180/mgm.2019.1 Published online by Cambridge University Press